

Article

# Aerodynamic and Structural Characteristics of a Centrifugal Compressor Impeller

T R Jebieshia <sup>1</sup>, Senthil Kumar Raman <sup>2</sup> and Heuy Dong Kim <sup>2,\*</sup><sup>1</sup> FMTRC, Daejoo Machinery, Daegu 42721, Korea<sup>2</sup> Department of Mechanical Engineering, Andong National University, Andong 36729, Korea

\* Correspondence: kimhd@anu.ac.kr

Received: 21 July 2019; Accepted: 14 August 2019; Published: 19 August 2019



**Abstract:** The present study focuses on the aerodynamic performance and structural analysis of the centrifugal compressor impeller. The performance characteristics of the impeller are analyzed with and without splitter blades by varying the total number of main and splitter blades. The operating conditions of the compressor under centrifugal force and pressure load from the aerodynamic analysis are applied to the impeller blade and hub to perform the one-way Fluid–Structure Interaction (FSI). For the stress assessment, maximum equivalent von Mises stresses in the impeller blades are compared with the maximum allowable stress of the impeller material. The effects of varying the pressure field on the deformation and stress of the impeller are also calculated. The aerodynamic and structural performance of the centrifugal compressor at 73,000 rpm are investigated in terms of the efficiency, pressure ratio, equivalent von Mises stress, and total deformation of the impeller.

**Keywords:** Fluid–Structure Interaction (FSI); flow characteristics; impeller; performance analysis; compressor blade; von Mises stress

## 1. Introduction

Impellers are required to be designed to withstand the centrifugal force due to the rotation of rotor assemblies and the pressure forces due to the three-dimensional viscous fluid flow inside blade channels [1,2]. Both the inertial forces due to rotation and hydrodynamic forces due to the flow result in stress acting on the impeller blade surfaces. Currently, power cycle systems demand higher pressurizing components with a wider operating range. Moreover, impeller with reduced weight can operate at high speed with lesser input power. Designing an impeller to meet such prerequisites with reliability is a challenging task and requires a coupled fluid–structure interaction analysis. The centrifugal and Coriolis forces generated in the centrifugal compressor impeller can be determined using Computational Fluid Dynamics (CFD) analysis, and the stresses acting on the impeller can be determined using the Fluid–Structure Interaction (FSI) analysis. The stress values obtained from the analysis are then applied to perform the pre-stressed analysis.

The FSI analyzes the behavior of the structure under the action of the flow field, and it can be one-way or two-way depending on the transfer of the analysis results. In the one-way FSI, the CFD results are transferred to the structural analysis by one-way coupling, while in two-way FSI, the deformations in the structure obtained from the transfer of the CFD results are fed back to the CFD environment, to determine the deviation in the flow created as a result of the structural deformation [3]. Several researchers [4–8] studied the effect of FSI on radial forces, pressure distribution, equivalent stress, and rotor deflection in a centrifugal compressor and pump. Zhao et al. [9] suggested that the complete compressor performance analysis should involve both fluid and solid mechanics and found that the fluid pressure influences the von Mises stress significantly. Schneider et al. [10] quantitatively analyzed the distribution of stress and deformation in the impeller of the multistage

pump. Kobayashi et al. [11] investigated a mixed-flow pump with an unshrouded impeller by one-way coupled FSI, and the distribution of stress on the impeller was obtained. Piperno et al. [12] concluded that to ensure the safe operation of a rotating structure for every flow rate, the analysis of stress and deformation on the impeller in the unstable operation region needs to be solved by the consideration of FSI. Kang and Kim [13] pointed out that structural safety needs to be evaluated because the impeller receives fluid pressure load and centrifugal force during the operation.

In the system of FSI, there are some interactions between two different physical fields on the coupling interface. Field force, which interacts on the structure surface, has an influence on the movement of the structure, and the deformation of the structure also changes the fluid calculation area and the boundary conditions, which affect the flow field [14]. Thus, it becomes necessary to analyze the effects of the impeller blade shape on its aerodynamic performance and structural safety by using FSI. To evaluate the structural integrity and stability of the impeller during the lifespan, a fluid–solid interaction is required to assess the stresses. Similarly, to acquire a superior design, a reasonable compromise between the aerodynamic, stress, and rotor dynamics is needed to be found. Depending on the mechanical design criteria, the model with the lowest overall von Mises nodal stress has been sought to determine the best impeller design [5,15]. The structural part deforms due to the pressure or temperature load from the fluid domain. One-way coupled FSI analysis is performed using the pressure load results from CFD. The pressure load is imposed in carrying out the pre-stressed structural analysis. The present study focuses on the flow characteristics, the aerodynamic performance analysis, and the structural safety of the centrifugal compressor impeller.

## 2. Methodology

The commercial software ANSYS 19.2 was used for the present one-way FSI steady static analysis. The three-dimensional model of the centrifugal compressor impeller was generated in the BladeGen feature of Workbench using the design parameters given in Table 1. The impeller meridional profile distribution is shown in Figure 1. The fluid field was numerically simulated by the CFX program to obtain the distribution of pressure using the Finite Volume Method (FVM). Once the mesh was created in TurboGrid, the initial parameter defining the aerodynamic simulation was set in CFX-Pre and then solved in CFX-Solver. The total pressure and the total temperature at the inlet were set to 1.0 bar and 298.16 K, respectively. The operating conditions were within the thermodynamic region where the ideal gas law is valid, and hence, the working fluid, air, was considered as an ideal gas. The designed mass flow rate was set at the outlet for steady-state simulation. No slip boundary conditions were assumed at the solid walls of the impeller domain; the total temperature and pressure conditions at the impeller inlet were set; and appropriate constraints on displacements were applied to the FEA model. The rotational speed was applied with respect to the Z-direction in terms of the number of Revolutions Per Minute (spin speed, RPM).

The structured mesh was generated with the TurboGrid tool, and the computational domain with mesh is shown in the Figure 2. Grids were refined near the wall regions such that  $Y^+$  was less than 5 to resolve the solution accurately. After the mesh independence study, for the twelve-blade configuration, it was found that for a further increment in the mesh after 1 million, the difference in the efficiency results was less 0.01 %, as shown in Figure 3. Hence, the computational domain with 1 million meshes was used in this study for the 12-blade configuration. Similarly, for 6-, 8-, 10-, 15-, and 20-blade configuration, the domains with 0.74-, 0.78-, 0.82-, 1.2- and 1.3-million meshes, respectively, were used.

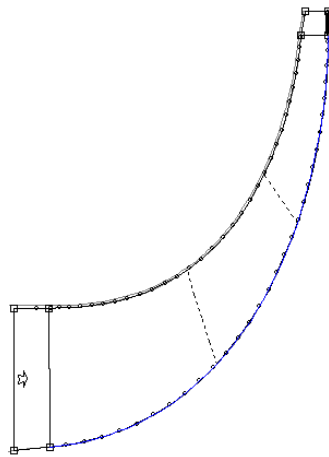


**Figure 1.** Meridional section of blade profile of the impeller.

The  $K-\omega$  shear-stress-transport turbulence model, which blends the  $k-\omega$  model near the boundary layer region and the  $k-\epsilon$  model away from the boundary layer region, was adapted in this study to approximate the turbulence parameters. The numerical iteration was considered to be a converged solution after the residuals of the equations fell below  $10^{-4}$ .

**Table 1.** Design parameters of the centrifugal compressor impeller.

Parameters	Details
Rotational velocity	73,000 rpm
Impeller outer diameter	123 mm
Impeller width	3.6 mm
Impeller suction diameter	51.4 mm
Impeller hub diameter	15 mm
Discharge diameter	129.16 mm
Discharge width	2.99 mm
Length in axial direction	86.63 mm
Axial length of main blades	36.60 mm
Axial length of splitter blades	17.10 mm

A numerical three-dimensional solid model of the entire impeller was created in Design Modeler, and for FE analysis, the material was assumed to be isotropic, i.e., the material had the same elastic properties in all directions. For structural analysis, Grade 5 titanium alloy, Ti-6Al-4V(G5), was considered as the impeller material, and the corresponding material property details are listed in Table 2. The temperature effects were neglected as it was considered that the temperature along the blades was constant. The cylindrical hub surface was locked against radial and tangential movements, i.e., nodes between the impeller and axle shaft were fully constrained. The blades were firmly attached to the impeller hub along with their inner profiles.

**Table 2.** Material property details of titanium alloy Ti-6Al-4V(G5).

Material Property	Details
Modulus of elasticity	114 GPa
Poisson's ratio	0.33
Density	4430 kg/m <sup>3</sup>
Tensile strength, ultimate	1170 MPa
Tensile strength, yield	1100 MPa

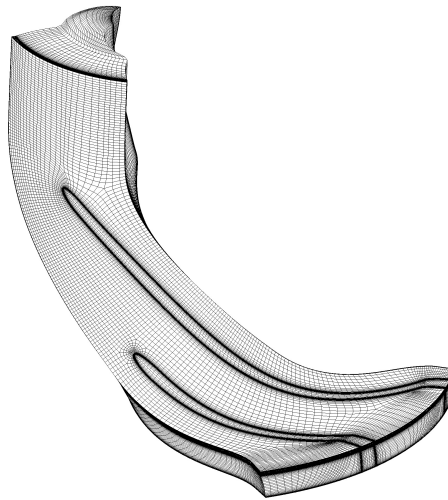


**Figure 2.** Computational domain with meshes.

The surface pressure field on the impeller blades obtained from CFD analysis can be directly applied as the loading using an interface to connect fluid flow and structural strength analyses. To determine the fluid pressure load on the structure, the impeller surface was set as the fluid–structure interaction surface (fluid–solid interface). Isentropic efficiency, the total pressure ratio, and other meridional profile details of the impeller were estimated to identify the performance of the compressor impeller with different blade numbers. Based on FSI, von Mises stress and total deformation due to the pressure loads on the blade surfaces from the aerodynamic analysis with and without rotational velocity were analyzed by the static structural module. In the static structural module, the strength of the impeller was assessed by the von Mises stress criterion.

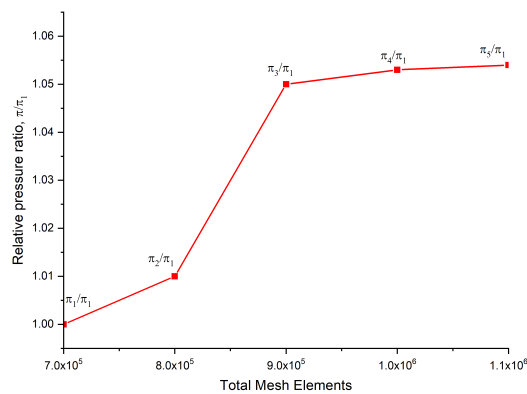


**Figure 3.** Mesh independence test for the impeller.

### 3. Results and Discussion

Performance analysis and FSI of a centrifugal compressor impeller were carried out, and the results are presented in this section.

#### 3.1. Aerodynamic Performance

The efficiency and pressure ratio of the impeller with and without splitter blades for the different number of blade cases are shown in Figure 4. The camber shape and thickness profile of the splitter blades were inherited from the corresponding ones of the main blade. For the same blade number,

the inclusion of splitter blades increased the pressure rise and efficiency. At a lower blade number, the influence of splitter blades on the pressure rise was more pronounced.

Aerodynamic performance of the splitter and without splitter configuration at the same rotational speed is tabulated in Table 3. At a constant mass flow rate of 0.3 kg/s, the total pressure ratio and the efficiency of splitter blades were higher than the without configuration case. However, higher input power was required for the splitter case than the respective non-splitter case. More power was required to move the additional splitter blade surface, which generated more pressure and viscous forces.

### 3.1.1. Without Splitter Blades

The blade-to-blade view of the velocity vectors at 50% span for blade numbers of 6, 15, and 20 is shown in Figure 5a–c, respectively. A re-circulation region with low velocity was formed at the pressure side for the configuration with six blades. This region vanished on increasing blade number due to a reduction in the flow passage, which made it more streamlined. The peak velocity of 340 m/s was formed near the trailing edge of the suction side in the six-blade configuration. On increasing the blade number, this maximum velocity region moved upstream. The configuration with 15 blades having the highest pressure rise implied a relatively more uniform velocity distribution.

The meridional contour of entropy for different configurations is shown in Figure 6. The maximum entropy generation occurred in the configuration with 20 blades, while the difference between the six and 15 configurations was negligible. The entropy was generated due to re-circulation and frictional losses. Even though the higher blade number made the flow more streamlined, more blades led to more frictional losses, which in turn resulted in higher entropy. The circumferential pressure contour distribution at the trailing edge for a different number of blades is shown in Figure 7. The distortion in the circumferential pressure distribution decreased as the blade number increased. For the configuration with 15 blades, the high-pressure region was greater, which corresponds to the higher pressure rise in Figure 7b.

### 3.1.2. With Splitter Blades

The effect of adding splitter blades to the current impeller design is studied and presented in this section. The blade-to-blade view of velocity vectors at 50% span, the meridional contour of entropy, and the circumferential pressure contour distribution at the trailing edge for the different numbers of blade are shown in Figures 8, 9, and 10, respectively.

The inclusion of splitter blades streamlined the flow after a 50% blade length and prevented the formation of the low-velocity re-circulation region on the pressure side for the six-blade configuration, as shown in Figure 8a. However, small re-circulation formed at the suction side of the splitter blade due to higher flow incidence at the splitter blade leading edge. On increasing the blade number, the flow incidence angle at the splitter leading edge decreased, and the re-circulation region moved downstream.

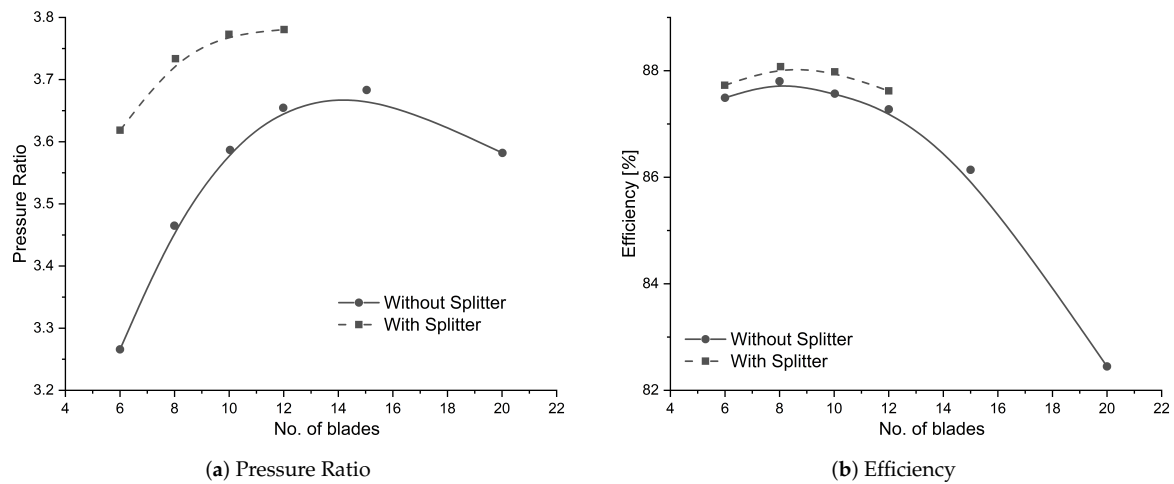


Figure 4. Performance characteristics.

The maximum entropy generated was decreased from 136 KJ/kg-K to 130 KJ/kg-K upon the inclusion of splitter blades, as shown in Figures 6 and 9. This maximum entropy region formed at the curvature of the meridional profile for the configuration without the splitter and moved downstream in the splitter configuration. The inclusion of splitter blades decreased the distortion in the circumferential pressure distribution, as shown in Figure 10. This even distribution of circumferential pressure with higher pressure corresponded to the high-pressure rise of splitter configuration. The magnitude of the high pressure region was decreased for the 12-blade configuration, as shown in Figure 10c.

Table 3. Compressor performance results.

	Blade #8		Blade #10		Blade#12	
	No Splitter	Splitter	No Splitter	Splitter	No Splitter	Splitter
Rotation Speed (radian s <sup>-1</sup> )	-7644.54	-7644.54	-7644.54	-7644.54	-7644.54	-7644.54
Mass Flow Rate (kg s <sup>-1</sup> )	0.3000	0.3000	0.3000	0.3000	0.3000	0.3000
Inlet Volume Flow Rate (m <sup>3</sup> s <sup>-1</sup> )	0.2361	0.2512	0.2427	0.2536	0.2464	0.2535
Input Power (W)	40,969.9	46,516.6	43,550.8	47,486.3	45,133.3	47,743.9
Work Input Coefficient	0.6663	0.7109	0.6892	0.7189	0.7034	0.7230
Total Pressure Ratio	3.4691	3.7317	3.5866	3.7743	3.6542	3.7771
Total Temperature Ratio	1.4897	1.5225	1.5065	1.5284	1.5169	1.5313
Total Isentropic Efficiency (%)	87.8024	88.0925	87.5507	88.0186	87.2671	87.6186
Total Polytropic Efficiency (%)	89.7042	90.0684	89.5477	90.0228	89.3419	89.6915

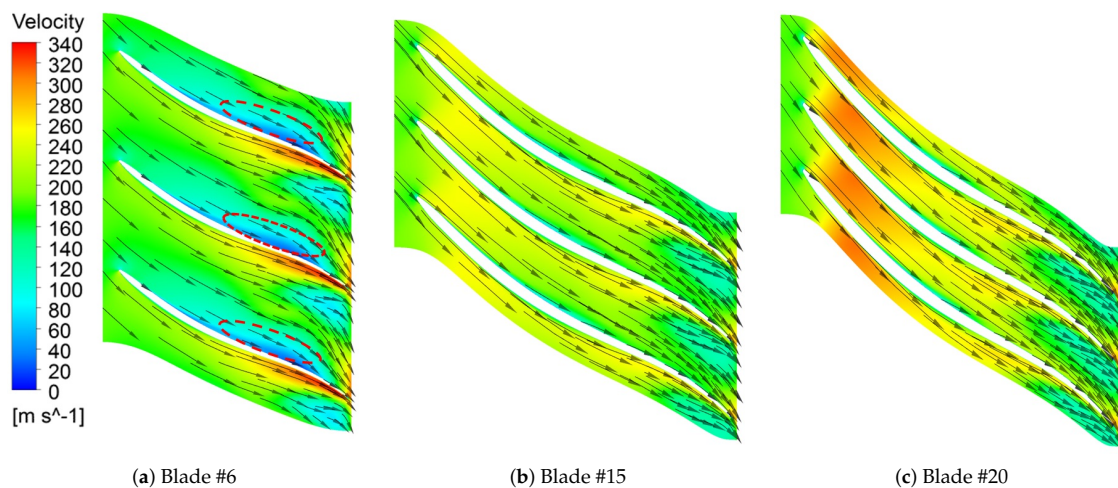


Figure 5. Velocity vectors' 50% span. The re-circulation zone is marked with the dashed circle.

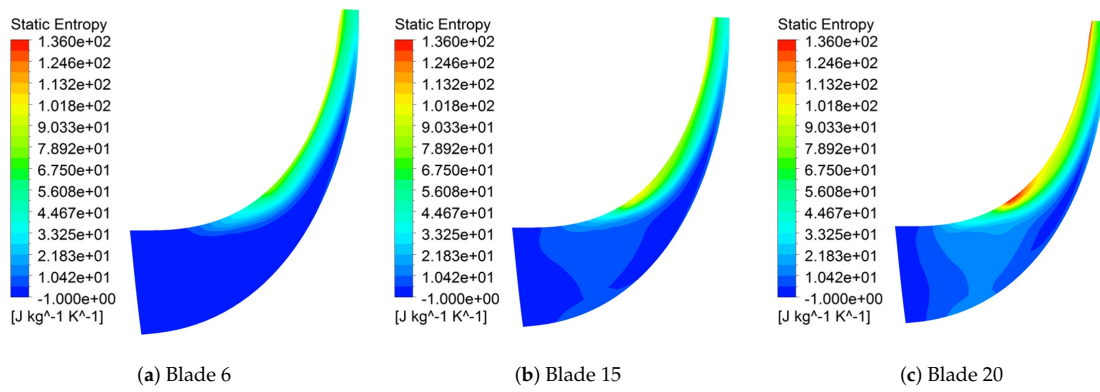


Figure 6. Entropy contour on the meridional surface.

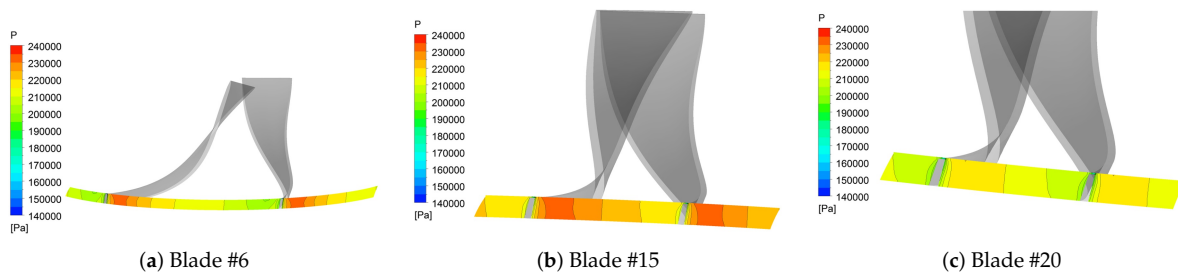


Figure 7. Pressure contour at the trailing edge.

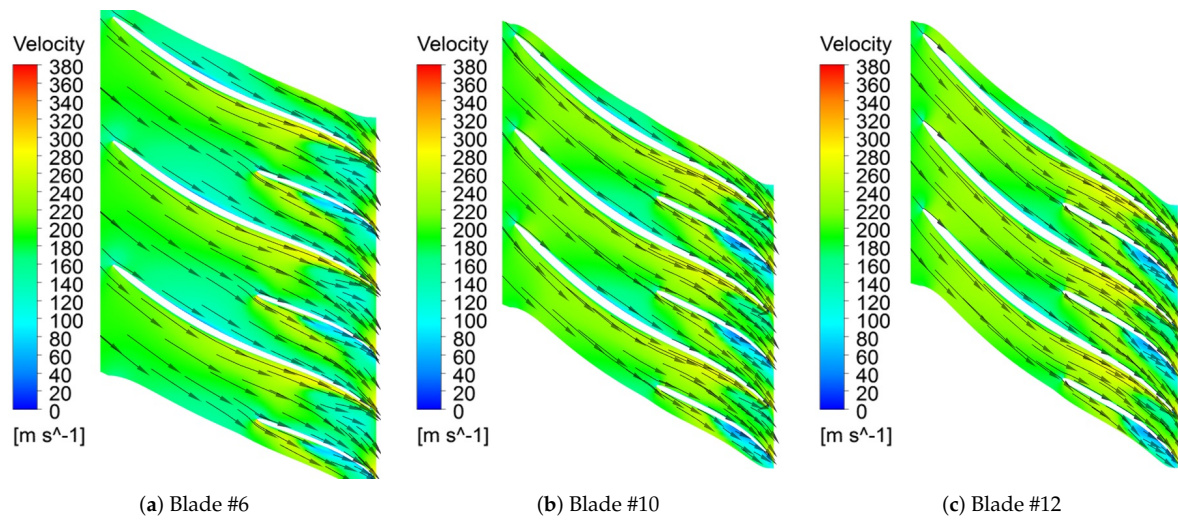


Figure 8. Velocity vectors' 50% span, with splitter blade.

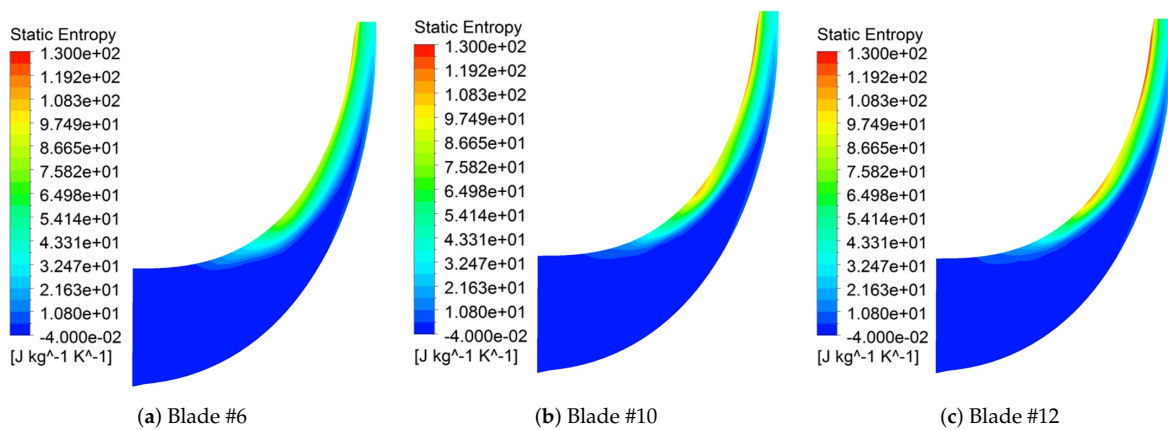


Figure 9. Entropy contour on the meridional surface, with splitter blade.

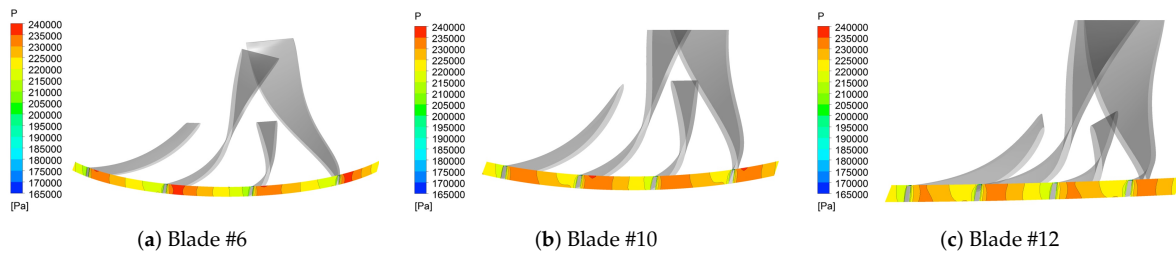


Figure 10. Pressure contour at the trailing edge, with splitter blade.

### 3.2. Fluid–Structure Interaction

A set of main and splitter blades was used to study the effect of fluid pressure on the deformation and stress of the impeller blades. The total deformation and equivalent von Mises stress with and without rotation were calculated for three cases, Blade Set Numbers 8, 10, and 12. The total deformation of the impeller under the FSI condition is shown in Figures 11 and 12.

It was evident from the results that the maximum displacement occurred at the end of the impeller blade leading edge for both cases. As the impeller rotated, the deformation increased several times at the downstream blade surface away from the hub.

For the static case, it is clear from Figure 13 that the maximum von Mises stress occurred at the leading edge of the main blade at the interface of the impeller blade and hub. Under the action of the centrifugal force and aerodynamic force, the maximum equivalent stress of the impeller was located at the trailing edge of the splitter blade (Figure 14). As the number of blades increased, the general trend of the maximum von Mises stress was decreasing for both the with and without rotation cases, except the case of Blade Number 12 with rotation (Figures 13 and 14). The location of the maximum total deformation and equivalent von Mises stress was similar to that in the literature [13]. These stress concentrated areas were vulnerable to different types of failures. The maximum equivalent von Mises stress appearing in the impeller structure from the static structural analysis was much lower than the yield stress for all the cases, and it can be inferred that the structure was safe and could operate for a wide range of operating conditions.

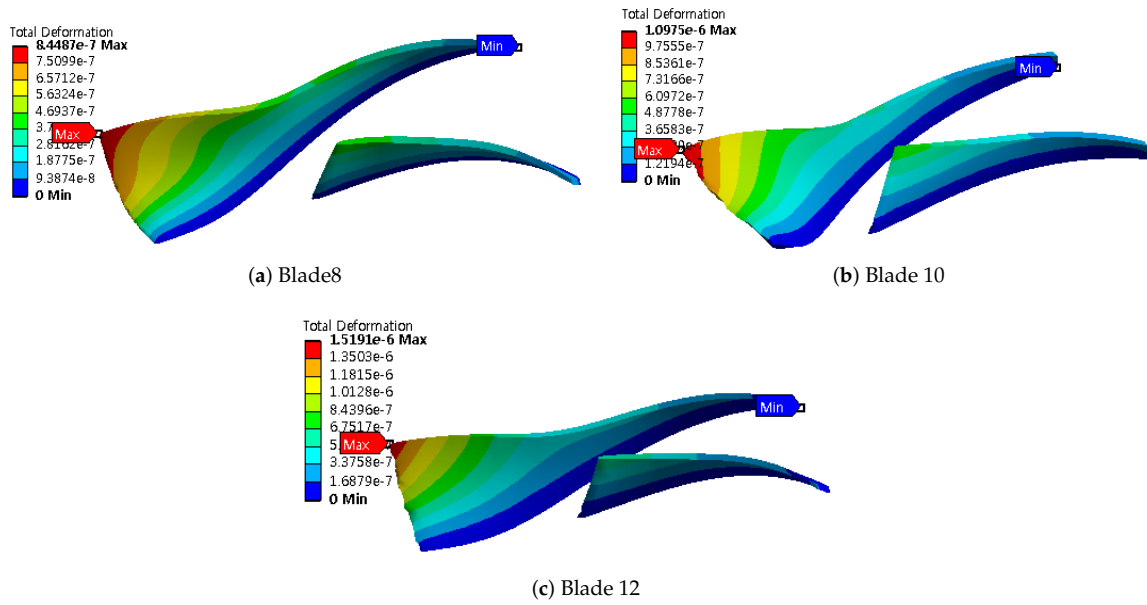


Figure 11. Total deformation.

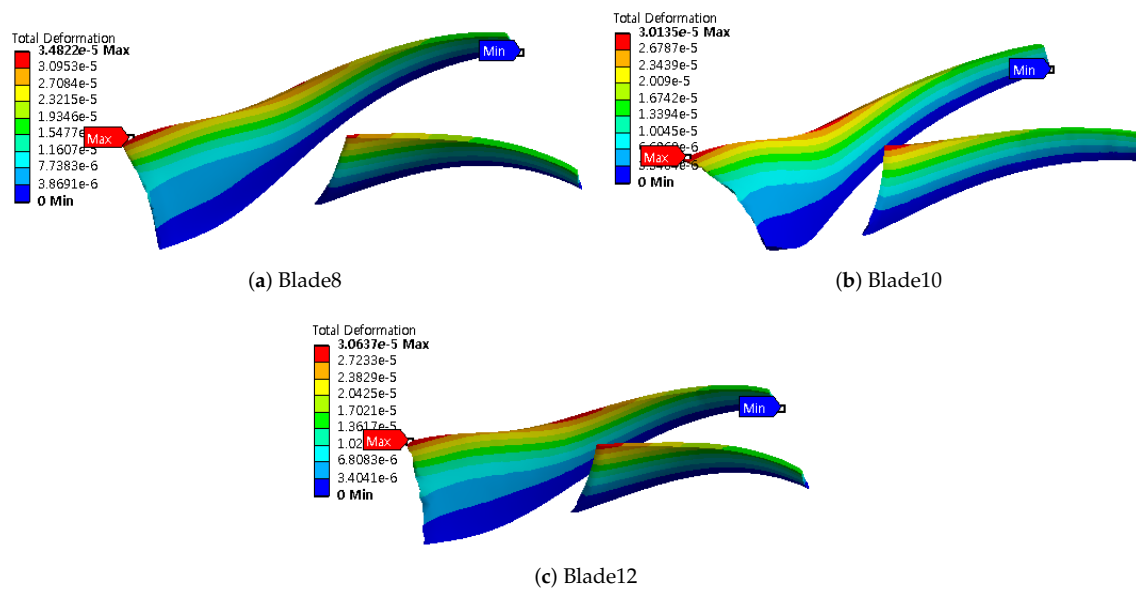


Figure 12. Total deformation with rotation.

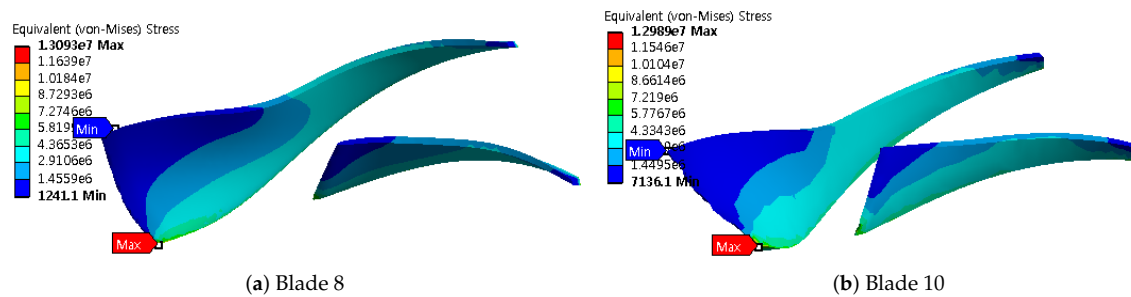


Figure 13. Cont.

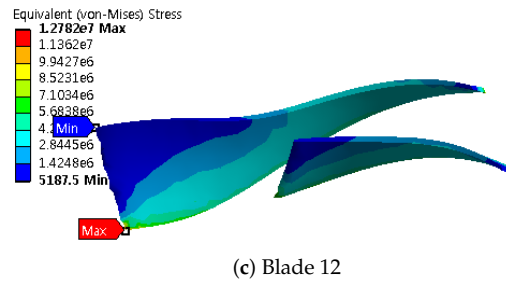


Figure 13. Equivalent von-Mises stress.

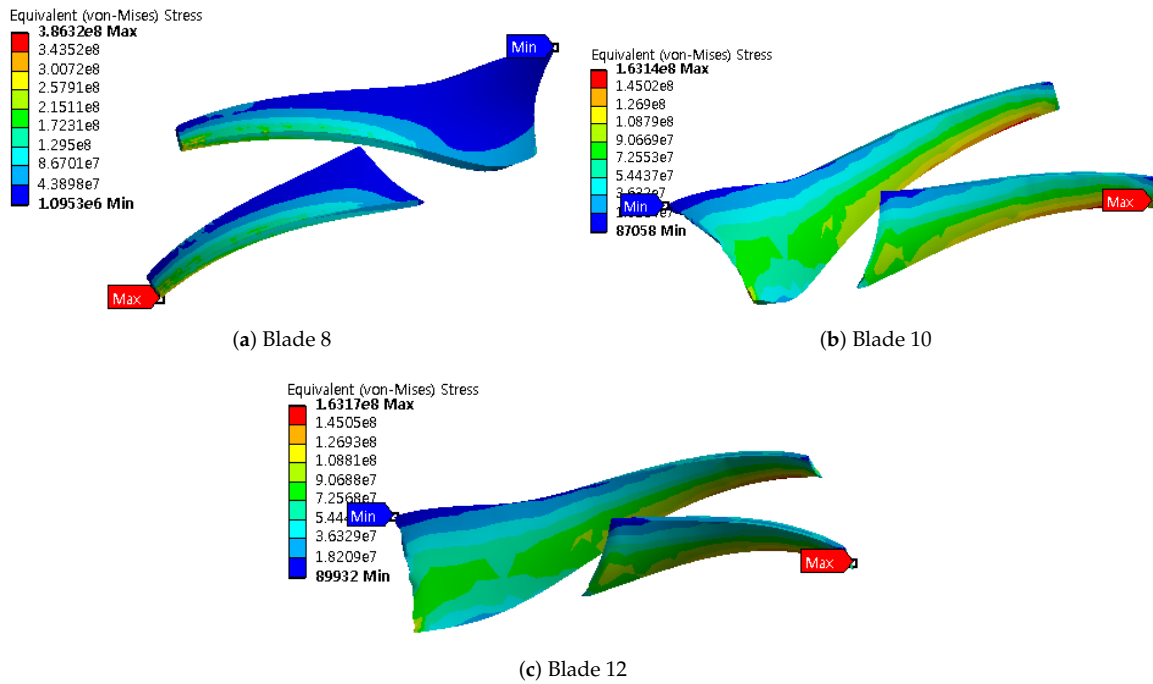


Figure 14. Equivalent von Mises stress with rotation.

#### 4. Conclusions

The main conclusions obtained from the present study are summarized in this section. The aerodynamic characteristics of a centrifugal compressor impeller were analyzed through CFD analysis. In order to obtain the distribution of total deformation and equivalent stress on the impeller surface, the coupled solution of the flow field and structural response of the impeller was established. Aerodynamic characteristics and structural safety assessments were carried out through CFD and FSI analysis on centrifugal compressors. This can be applied to the optimal design for the improvement of compressor efficiency.

In the without splitter configuration, a re-circulation region formed near the pressure side, and upon increasing the blade number, this region vanished. The inclusion of splitter blades removed the formation of the low-velocity region, as well as more evenly distributed the circumferential pressure distribution. The addition of splitter blades increased the efficiency and pressure rise with more input power requirement.

A coupled solution of the flow field and structural response of the impeller was proven by the use of a one-way coupling method. This method allowed for the study of the flow characteristics and the quantitative analysis of the structural performance of the centrifugal compressor impeller. The maximum displacement under the flow pressure distribution occurred at the end of impeller blade leading edge for both with and without rotational velocity. The stress concentrated areas of the impeller blades were near the hub region and were prone to damage. It was concluded that the

structure was safe as the maximum von Mises stress was much lower than the yield stress of the impeller material.

**Author Contributions:** Investigation, S.K.R., and T.R.J.; Methodology, T.R.J., and S.K.R.; Project administration, H.D.K.

**Acknowledgments:** The authors are deeply grateful for the financial support of this study by the Korea Institute of Energy Technology Evaluation and Planning (KETEP) and the Ministry of Trade, Industry & Energy (MOTIE) of the Republic of Korea (No. 20172010105200).

**Conflicts of Interest:** The authors declare no conflict of interest.

## References

1. Mojaddam, M.; Pullen, K. Optimization of a Centrifugal Compressor Using the Design of Experiment Technique. *Appl. Sci.* **2019**, *9*, 291. [[CrossRef](#)]
2. Bardelli, M.; Cravero, C.; Marini, M.; Marsano, D.; Milingi, O. Numerical Investigation of Impeller-Vaned Diffuser Interaction in a Centrifugal Compressor. *Appl. Sci.* **2019**, *9*, 1619. [[CrossRef](#)]
3. Benra, F.K.; Dohmen, H.J.; Pei, J.; Schuster, S.; Wan, B. A comparison of one-way and two-way coupling methods for numerical analysis of fluid-structure interactions. *J. Appl. Math.* **2011**, *2011*. [[CrossRef](#)]
4. Gu, Y.; Pei, J.; Yuan, S.; Xing, L.; Stephen, C.; Zhang, F.; Wang, X. Effects of blade thickness on hydraulic performance and structural dynamic characteristics of high-power coolant pump at overload condition. *Proc. Inst. Mech. Eng. Part A J. Power Energy* **2018**, *232*, 992–1003. [[CrossRef](#)]
5. Ying, Q.; Zhuge, W.; Zhang, Y.; Zhang, L. Design Optimization of A Small Scale High Expansion Ratio Organic Vapour Turbo Expander for Automotive Application. *Energy Procedia* **2017**, *129*, 1133–1140. [[CrossRef](#)]
6. Gong, C.D.; Lee, H.S.; Kim, I.K. Aerodynamic and Structural Design of A High Efficiency Small Scale Composite Vertical Axis Wind Turbine Blade. *Trans. KSAS* **2011**, *39*, 758–765. [[CrossRef](#)]
7. Drewczynski, M.; Solution, G.E.; Rzakowski, R. A stress analysis of a compressor blade in partially blocked inlet condition. *Proc. IMechE Part G J. Aerosp. Eng.* **2015**, 1–19. [[CrossRef](#)]
8. Kang, H.S.; Kim, Y.J. Optimal design of impeller for centrifugal compressor under the influence of one-way fluid-structure interaction. *J. Mech. Sci. Technol.* **2016**, *30*, 3953–3959. [[CrossRef](#)]
9. Zhao, H.; Deng, Q.; Zheng, K.; Zhang, H.; Feng, Z. Numerical Investigation on the Flow Characteristics of a Supercritical CO<sub>2</sub> centrifugal compressor. In Proceedings of the ASME Turbo 2014: Turbine Technical Conference and Exposition, Düsseldorf, Germany, 16–20 June 2014; pp. 1–10. [[CrossRef](#)]
10. Schneider, A.; Will, B.C.; Böhle, M. Numerical evaluation of deformation and stress in impellers of multistage pumps by means of fluid structure interaction. In Proceedings of the ASME 2013 Fluids Engineering Division Summer Meeting, Incline Village, NV, USA, 7–11 July 2013; pp. 1–10.
11. Kobayashi, K.; Ono, S.; Harada, I.; Chiba, Y. Numerical Analysis of Stress on Pump Blade by One-Way Coupled Fluid-Structure Simulation. *J. Fluid Sci. Technol.* **2010**, *5*, 219–234. [[CrossRef](#)]
12. Piperno, S.; Farhat, C.; Larroturou, B. Partitioned procedures for the transient solution of coupled aeroelastic problems Part I: Model problem, theory and two-dimensional application. *Comput. Methods Appl. Mech. Eng.* **1995**, *124*, 79–112. [[CrossRef](#)]
13. Kang, H.S.; Kim, Y.J. A study on the multi-objective optimization of impeller for high-power centrifugal compressor. *Int. J. Fluid Mach. Syst.* **2016**, *9*, 143–149. [[CrossRef](#)]
14. Gong, B.L.; Jia, X.J.; Wang, G.C.; Liu, Z.W. Study on application of CAE in a centrifugal compressor impeller. *Adv. Mater. Res.* **2013**, *787*, 594–599. [[CrossRef](#)]
15. Lee, K.; Huque, Z.; Kommalapati, R.; Han, S.E. The Evaluation of Aerodynamic Interaction of Wind Blade Using Fluid Structure Interaction Method. *J. Clean Energy Technol.* **2014**, *3*, 270–275. [[CrossRef](#)]

